RSC Advances

ROYAL SOCIETY OF CHEMISTRY

www.rsc.org/advances

Journal Name

RSCPublishing

ARTICLE

Enhanced cycling stability of silicon anode by *in situ* polymerization of poly(aniline-co-pyrrole)

Cite this: DOI: 10.1039/xoxxoooooox

Qingtao Wang,* Ruirong Li, Dong Yu, Xiaozhong Zhou, Jian Li and Ziqiang Lei*

Received ooth January 2012,
Accepted ooth January 2012

DOI: 10.1039/xoxxoooooox

www.rsc.org/

The application of silicon-based Li-ion battery anode is limited by the poor cycling stability associated with its large volume changes during charging and discharging processes. Here we report a facile solution process to fabricate silicon composite anodes by encapsulating Si nanoparticles with *in situ* polymerized aniline and pyrrole copolymer. The copolymer matrix can accommodate the great volume changes of Si during the cycling process. Therefore, the as-prepared Si/poly(aniline-co-pyrrole) composite electrodes successfully achieve higher capacity and better cycling performance than the bare nano-Si anode. The specific capacity of the composite electrode retains 637 mAh g^{-1} after 50 cycles.

Introduction

The grid-scale energy storage systems and electric vehicles require developing next generation lithium-ion batteries with high energy density and long cycle life.[1] Currently, the theoretical specific capacity of commercial graphite anode is 370 mAh g^{-1},[2] so it does not meet the need of high energy storage. Silicon has been considered as a promising alternative anode material due to its high specific capacity (4200 mAh g^{-1}) and low delithiation potential (~0.4 V versus Li/Li^+).[3] However, the active Si material will be damaged and lose the contact with current collector because of the tremendous volume expansion during cycling (more than 300%).[4] Furthermore, silicon is a semiconductor material and its bulk conductivity as low as 6.7×10^{-4} S/cm.[5] In recent years, the silicon with nanostructure has been extensively studied and considerable progress has been made, for example, nanoparticles,[6] nanowires,[7] nanotubes[8] and nanofilms.[9] In addition, Si/carbon[10] and Si/metal[11] composite electrode showed good performance because the composite could accommodate the severe volume expansion. Although the electrochemical performance has improved greatly, the inherent volume change is still the barrier for commercialization of silicon-based anodes.

Conducting polymers have various applications in electronics,[12] batteries[13] and supercapacitors[14] because of its good environmental stability. Recently, conducting polymer has been used to make Si/conducting polymer composite anode, which showed improved cyclability and rate performance. For example, Cai et al.[15] have synthesized the Si/polyaniline (PANI) composite anode, which showed stable cyclability and improved rate performance because the nest-like PANI enhanced the conductivity of the whole composite electrode and accommodated the large volume expansion of Si. Yao et al.[16] have reported that the poly(3,4-ethylenedioxythiophene) (PEDOT) coated Si nanowires anode material was synthesized and the improvement in cycling stability is attributed to the conductive coating maintaining the mechanical integrity of the cycled Si material, along with preserving electrical connections between nanowires.

In this work, a novel Si/poly(aniline-co-pyrrole) (Si/PANI-PPy) composite anode material was prepared by *in situ* chemical oxidation polymerization method. The copolymer matrix could act as an effective component that accommodates the great volume changes of Si during the cycling process. Therefore, the Si/PANI-PPy composite electrode achieved high capacity and stable electrochemical cycling.

Experimental

Preparation of the Si/PANI-PPy composite anode material

Si/PANI-PPy composite was synthesized by an *in situ* chemical oxidation polymerization method. The dopant was sodium p-toluenesulfonate and the oxidant was ammonium persulfate ($(NH_4)_2S_2O_8$). The molar ratio of pyrrole to aniline was 1:1 and the monomer to dopant was 3:1, the monomer to oxidant was 1:3. Typically, Si nanopowder (Shanghai Chao Wei Nano Technology Co., Ltd.) was dispersed in an aqueous solution of sodium p-toluenesulfonate, pyrrole and aniline. The pH of the solution was adjusted to 2 by hydrochloric acid. Then, the aqueous solution of $(NH_4)_2S_2O_8$ was slowly added with continuous stir. The reaction mixtures were then kept under the same conditions for 4 h at room temperature. The total dark green mass was filtered, and then washed thoroughly with distilled water to remove the ammonium persulfate to a large extent. Finally, the dark green mass was dried at 60 ℃ for 12 h under vacuum.

Material characterizations

The morphology of the as-prepared Si/PANI-PPy composite was observed using field emission scanning electron microscopy (Carl Zeiss Ultra Plus) and transmission electron microscopy (TEM, FEI TECNAI TF20). Fourier transformation

infrared (FTIR) spectra of the samples were measured on a Digilab Merlin FTS 3000 spectrometer in the transmission mode. Powder X-ray diffraction (XRD) patterns were obtained on a RigaKu D/max 2400 diffractometer with Cu K-alpha radiation. Thermal gravimetric analysis (TGA) was taken on a PrekinElmer Pyris Diamond instrument at 10 ℃/min in air atmosphere.

Electrochemical measurements

CR2025 coin cells were assembled to test the electrochemical performance of the Si/PANI-PPy composite. The testing electrodes were prepared by coating a slurry on cooper foil substrate. The slurry consists of 70 wt% active material of Si/PANI-PPy, 20 wt% conducting additive of carbon black, and 10 wt% binder of Sodium carboxymethyl cellulose (NaCMC). The cells were assembled in an Ar-filled glove box with a lithium foil as the counter electrode and a Celgard 2325 microporous film as the separator. The electrolyte was composed of 1 M $LiPF_6$ in ethylene carbonate (EC)/ethylmethyl carbonate (EMC)/dimethyl carbonate (DMC) (1:1:1 by volume, Shenzhen Capchem Technology Co., Ltd.) and 3 vol% vinylene carbonate (VC).

The galvanostatic charge-discharge measurement was performed at a current density of 50 mA g^{-1} in the first two cycles and 100 mA g^{-1} in the rest of cycles using a battery testing system (LANHE CT2001A, Wuhan LAND electronics Co., Ltd.) in the voltage range of 0.02-1.5 V (vs. Li/Li^+). The capacity was calculated based on the whole Si/PANI-PPy composite as active mass. Cyclic voltammetry (CV) and electrochemical impedance spectroscopy (EIS) measurements were performed on an electrochemical work-station (Autolab PGSTAT128N, Metrohm, Switzerland) at room temperature. The CV measurements were carried out in the voltage range of 0.02-1.5 V (vs. Li/Li^+) at a scan rate of 0.1 mV s^{-1}. EIS measurements were measured with an alternating voltage of 5 mV over the frequency ranging from 10^5 to 10^{-2} Hz.

Results and discussion

Structure and morphology of the Si/PANI-PPy composite

The FTIR spectra of Si, PANI, PPy, PANI+PPy, PANI-PPy and Si/PANI-PPy composite are shown in Fig. 1. The characteristic peaks of PANI at 1584 and 1502 cm^{-1} are assigned to the C=C stretching vibration of quinoid and benzenoid rings, respectively.[17] The bands located at 1302, 1145 and 1240 cm^{-1} belonged to C–N, C=N, and $C–N^+$ (polaron structure of PANI), respectively.[18] The bands at about 1041 and 834 cm^{-1} are due to the aromatic C–H in-plane bending and the out-of-plane deformation in the 1, 4-disubstituted benzene ring. In the spectrum of PPy, the characteristic C=C and C-N stretching vibration in the ring of PPy at 1544 and 1460 cm^{-1}, are clearly visible. The broad band from 1250 to 1100 cm^{-1} with a maximum at 1173 cm^{-1} is attributed to the breathing vibration of the pyrrole ring.[18] The band at 1036cm^{-1} corresponds to the C–H in plane bending. The spectrum of the 1:1 PANI+PPy homopolymer mixture shows all the characteristic bands of both PANI and PPy.

For the spectrum of PANI-PPy, the bands are different from those of the 1:1 PANI+PPy homopolymer mixture. The quinonoid phenyl ring C=C stretch band of PANI at l584 cm^{-1} and the C=C stretching mode of PPy at l544 cm^{-1} have amalgamated to form a broader band from l690 to 1530 cm^{-1}. A similar spectrum has also been reported.[19] While in the spectrum of PANI+PPy, the corresponding peaks are superposition of l584 cm^{-1} and l544 cm^{-1}. Secondly, the para-substituted aromatic C-H out-of plane bending band of PANI at 834 cm^{-1} has greatly diminished in PANI-PPy FTIR spectrum. While in the spectrum of PANI+PPy, the corresponding peak is very strong. This observation is likely to be caused by the replacement of An units by Py units along the chains.[20] These observed differences support the view that besides pyrrole-pyrrole and aniline-aniline linkages, aniline-pyrrole linkages are most likely to be present. The spectrum of Si/PANI-PPy shows all the characteristic bands of both Si and PANI-PPy.

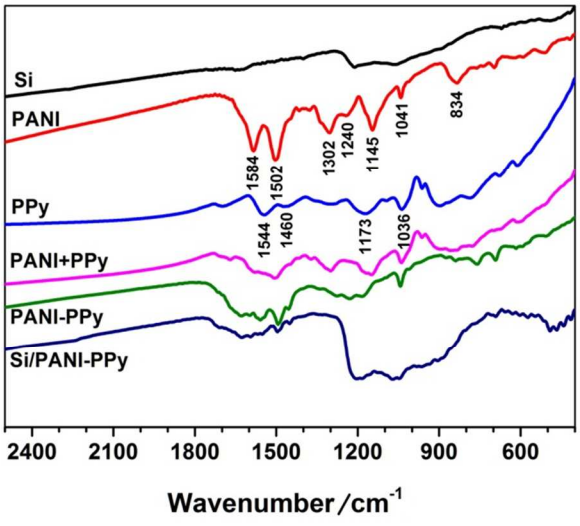

Fig. 1 The FTIR spectra of Si, PANI, PPy, PANI+PPy, PANI-PPy and Si/PANI-PPy composite.

The XRD pattern of purchased Si is given in Fig. 2. The main diffraction peaks at 2θ= 28.4°, 47.2°, 56.1°, 69.1° and 76.3° can be indexed as the (111), (220), (311), (400) and (331) planes of cubic Si crystallites (JCPDS card No. 27-1402), respectively. It is clearly seen that the XRD pattern of PANI-PPy composite shows the characteristic of an amorphous profile with a broad peak centered at 2θ= 20.1°. Compared with the XRD pattern of Si, the pattern of Si/PANI-PPy composite has no significant differences, which also indicate that the PANI-PPy coatings are amorphous.

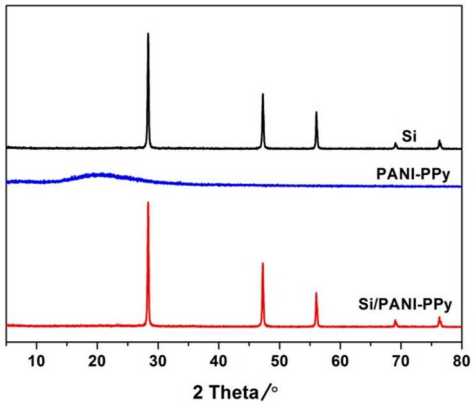

Fig. 2 The XRD patterns of Si, PANI-PPy and Si/PANI-PPy composite.

Fig. 3 shows scanning electron microscopy (SEM) images of the original Si nanoparticles (SiNPs) and Si/PANI-PPy composite. Typically, the diameter of spherical Si nanoparticles widely distributed from 20-160 nm (Fig. 3a). As the PANI-PPy was formed in the presence of the SiNPs, the SiNPs were embedded in the PANI-PPy copolymer. This is confirmed by SEM image of the Si/PANI-PPy composite (Fig. 3b). The irregular profile of SiNPs indicates that it were coated by the PANI-PPy copolymer.

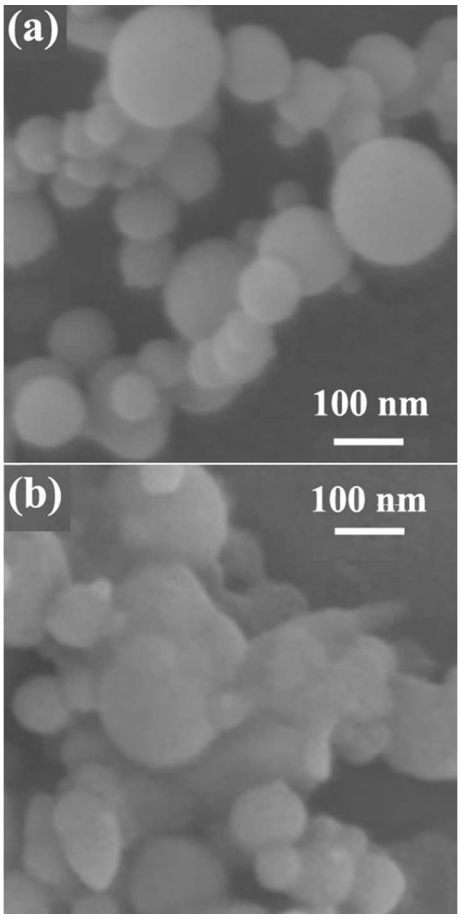

Fig. 3 The SEM images of Si nanoparticles (a) and Si/PANI-PPy composite (b).

To further confirm the structure of Si/PANI-PPy composite, transmission electron microscopy (TEM) image and scanning transmission electron microscopy (STEM) images are shown in Fig. 4. SiNPs appear to be embedded in the PANI-PPy copolymer matrix due to the *in situ* polymerization discussed above, as shown in Fig. 4a. Fig. 4b shows high angle annular dark field scanning transmission electron microscopy (HAADF-STEM) image of Si/PANI-PPy composite, from which we can obviously see bright sphere and gray region around it. In order to determine the composition, elemental linescan analysis was performed as shown in Fig. 4c. Linescan results indicate that the center bright sphere was assigned to silicon. The Si nanoparticle was encapsulated in the darker surroundings which were the PANI-PPy copolymer. As will be discussed later, the superior electrochemical performance of the Si/PANI-PPy composite electrode can be attributed to the advantages offered by the unique microstructure.

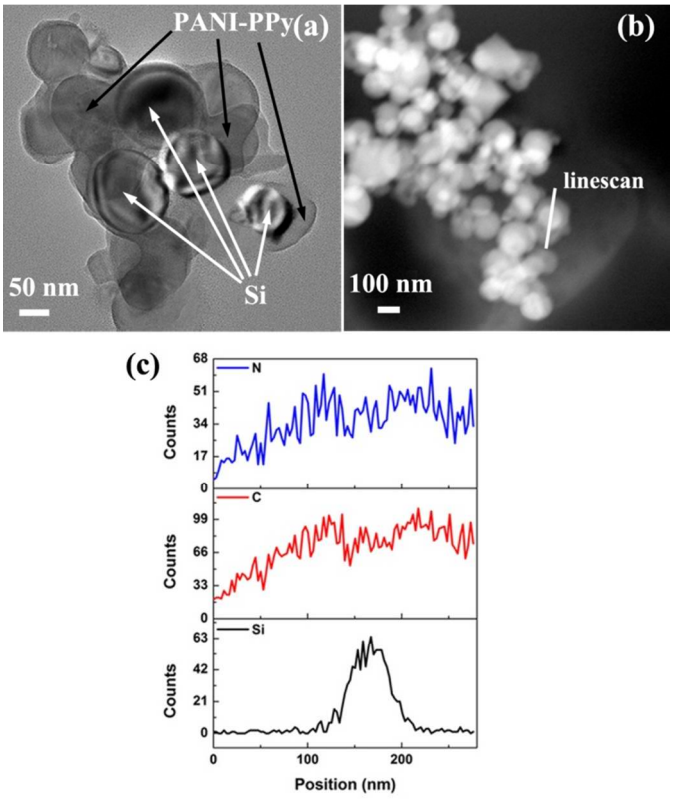

Fig. 4 The TEM (a) and HAADF-STEM (b) images of Si/PANI-PPy composite, along with the corresponding elemental linescan (c) from a single particle.

To determine the content of PANI-PPy copolymer in the Si/PANI-PPy composite, Thermal gravimetric analysis (TGA) was carried out in air. Fig. 5 shows the TGA curves of different mass ratio Si/PANI-PPy composite samples along with those of the bare Si and the PANI-PPy powders. PANI-PPy in the Si/PANI-PPy composite will be burnt and release gas (weight loss), while Si in the composite will be oxidized to SiO_2 (weight gain). Therefore, it is very hard to identify the weight loss region where PANI-PPy is burnt. The measured content of PANI-PPy in the Si/PANI-PPy composite was based on the minimum value of TGA curve. It was found that the amounts of PANI-PPy in the 1-Si/PANI-PPy, 2-Si/PANI-PPy, and 3-Si/PANI-PPy composites were 6.8 wt%, 14.7 wt%, and 27.5 wt%, respectively.

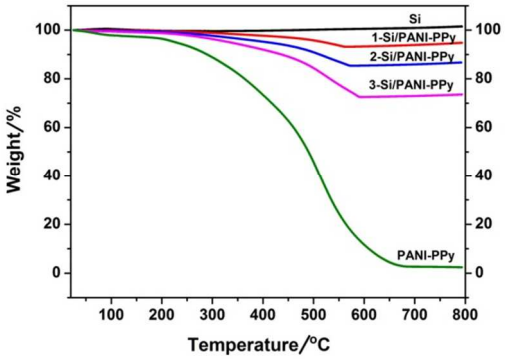

Fig. 5 The TGA curves of Si, PANI-PPy and different mass ratio of Si/PANI-PPy composite.

Electrochemical properties of the Si/PANI-PPy composite anode

The lithium intercalation and extraction cyclic performance of the 1-Si/PANI-PPy, 2-Si/PANI-PPy, and 3-Si/PANI-PPy composite anodes were tested and the results are shown in Fig. 6. The capacity values in this article were based on the mass of Si/PANI-PPy composites. For the 1-Si/PANI-PPy, 2-Si/PANI-PPy, and 3-Si/PANI-PPy composites, the initial discharge capacity is 2529 mAh g^{-1}, 2137 mAh g^{-1} and 1456 mAh g^{-1}. Over the 50 charge/discharge cycles, the capacity decreases to 470 mAh g^{-1}, 637 mAh g^{-1} and 185 mAh g^{-1}, respectively. It can be seen that the PANI-PPy copolymer contents affect the specific capacity and cycling stability of the Si/PANI-PPy composite anodes. With the copolymer content increasing from 6.8 to 14.7 wt%, the specific capacity of composite anodes increased from 470 to 637 mAh g^{-1}. The improved performance could be attributed to the better effect of accommodation with the increasing of PANI-PPy copolymer. However, when the content of the copolymer increased to 27.5 wt%, the specific capacity reduced to 185 mAh g^{-1}. It was ascribed to the introduction of excessive copolymer reduced the capacity of the entire Si/PANI-PPy composite. The 2-Si/PANI-PPy sample, with the measured content of PANI-PPy is 14.7 wt%, exhibits the highest capacity and cycling stability.

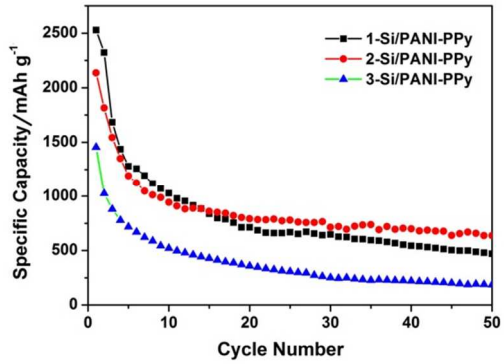

Fig. 6 The cyclic performance of different mass ratio Si/PANI-PPy composite anodes measured at a current density of 50 mA g^{-1} in the first two cycles and 100 mA g^{-1} in the rest of cycles.

The voltage profiles of the bare Si and 2-Si/PANI-PPy electrodes in the first cycle are shown in Fig. 7. The charge/discharge curves of the 2-Si/PANI-PPy composite electrode exhibited essentially the same features as the bare Si electrode. It can be seen that a long flat plateau around 0.1 V during the first discharge is observed, which was corresponding to crystalline Si reacted with Li to form amorphous Li_xSi.[21] The delithiation of Li_xSi during the charge process formed a plateau corresponding to delithiated amorphous silicon was formed.[22] The discharge capacities of bare Si and 2-Si/PANI-PPy composite electrode were 2963 and 2137 mAh g^{-1} with initial coulombic efficiencies of 82.4% and 77.9%, respectively. These low coulombic efficiencies in the first cycle was ascribed to the formation of dead Li, which was not dealloyed during the charge process because of disintegration of the electrode resulted from large volume change and the solid-electrolyte interface (SEI) layer formation on the surface of the electrode.[23]

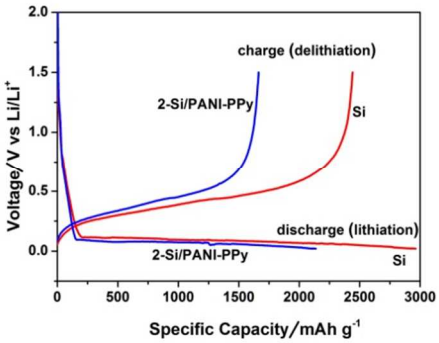

Fig. 7 The voltage profiles of the bare Si and 2-Si/PANI-PPy electrodes in the first cycle measured at a current density of 50 mA g^{-1}.

The capacity retention curve and coulombic efficiency (CE) curve of 2-Si/PANI-PPy composite anode are given in Fig. 8. For comparison purposes, the cycling behavior of the bare Si is also shown in Fig. 8. For the bare Si and 2-Si/PANI-PPy composites, the initial discharge capacity is 2963 mAh g^{-1} and 2137 mAh g^{-1}. Over the 50 charge/discharge cycles, the capacity decreases to 156 mAh g^{-1} and 637 mAh g^{-1}, respectively. It can be clearly seen that although the initial capacity of the 2-Si/PANI-PPy composite electrode is lower than that of the bare Si electrode, its cycling performance is much better than that of the bare Si. PANI-PPy can act as an effective component that accommodates the great volume changes during the cycling process. Therefore, PANI-PPy copolymer ensures the higher capacity and better cycling stability of the composite electrode.

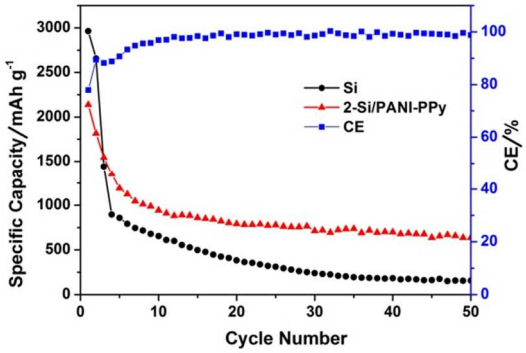

Fig. 8 The cyclic performance of Si and 2-Si/PANI-PPy anodes measured at a current density of 50 mA g^{-1} in the first two cycles and 100 mA g^{-1} in the rest of cycles, along with the coulombic efficiency curve of 2-Si/PANI-PPy anode.

The CV curves of 2-Si/PANI-PPy composite electrode are shown in Fig. 9. In the first cathodic branch, a broad cathodic peak observed between 0.6 and 0.8 V could be attributed to the formation of SEI film on the surface of the composite anode.[24] The peak disappears in the subsequent cycles. This phenomenon explains the low initial CE in the galvanostatic charging/discharging tests. Moreover, one additional cathodic peak appears near 0.17 V in the subsequent cycles, which is corresponding to the formation of Li-Si alloys.[25] During the first lithium ion extraction process, two broad anodic peaks occur at around 0.35 and 0.52 V corresponding to the phase transition from amorphous Li-Si alloys to amorphous Si.[16] After further cycles, the anodic peaks become broader and

stronger, which can be attributed mainly to the gradual breakdown of the crystalline silicon structure that depends on the migration rate of Li-ions into the silicon host and the rate of amorphous Li-Si alloy formation.[26]

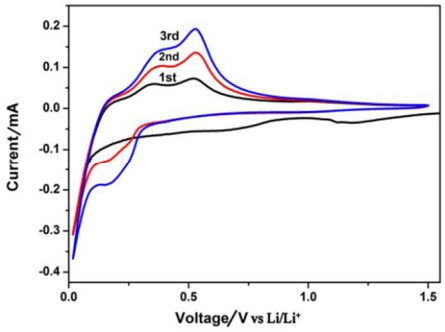

Fig. 9 The CV curves of 2-Si/PANI-PPy half-cell measured at scan rate of 0.1 mV s^{-1} between 0.02 and 1.5 V (vs Li/Li^+).

Fig. 10 shows the rate capability of the 2-Si/PANI-PPy composite anode at various current densities. The capacity of the 2-Si/PANI-PPy anode decreased from 2137 mAh g^{-1} to 699 mAh g^{-1} over 40 cycles at a current density of 100 mA g^{-1}. At the current density of 250, 500 and 1000 mA g^{-1}, the 2-Si/PANI-PPy anode could achieve a capacity of 440, 201 and 95 mAh g^{-1} after 40 cycles, respectively.

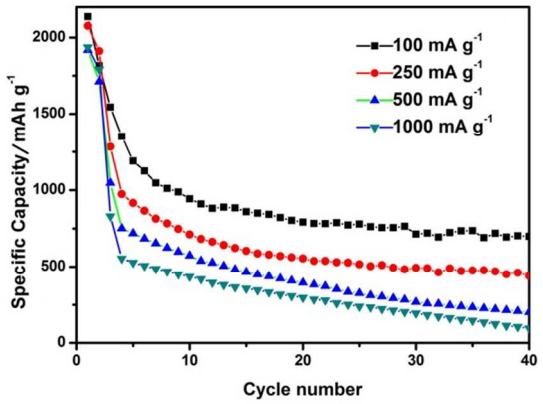

Fig. 10 The rate capability of the 2-Si/PANI-PPy composite anode.

The charge/discharge kinetics of the 2-Si/PANI-PPy composite anode was analyzed using electrochemical impedance spectroscopy (EIS). Fig. 11 shows the Nyquist plots of the cells with 2-Si/PANI-PPy composite anode. To maintain uniformity, the impedance analyses were done at a charged potential of 1.5 V after 3 and 30 cycles. The 0 times cycle's electrode were tested at a potential of 1.5 V. All of the impedance spectra have similar features with a medium-to-high frequency depressed semicircle and an inclined low-frequency line. According to previous researches, the inclined line in the low-frequency region represents the lithium diffusion impedance, while the depressed semicircle is attributed to the overlap between the SEI film and the interfacial charge transfer impedance.[27] The semicircle at high frequencies increased after 3 cycles in the case of 2-Si/PANI-PPy anode. It means that the total SEI and charge transfer resistances increase after 3 cycles. However, no obvious impedance increase was observed after 30 cycles, indicating limited growth of the SEI film during cycling.

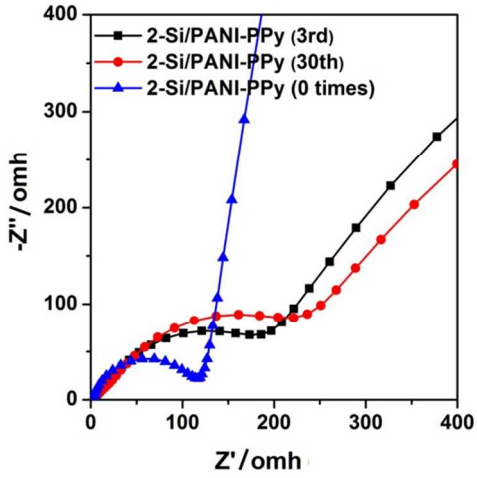

Fig. 11 The Nyquist plots of 2-Si/PANI-PPy composite anode measured with an alternating voltage of 5 mV from 10^5 to 10^{-2} Hz.

Conclusions

In summary, a facile solution process was developed to fabricate silicon-based Li-ion battery anode by encapsulating SiNPs with *in situ* polymerized PANI-PPy copolymer. The copolymer matrix could act as an effective component that accommodates the great volume changes of Si during the cycling process. Therefore, the Si/PANI-PPy composite electrode achieved high capacity and stable electrochemical cycling. The specific capacity of the composite electrode retained 637 mAh g^{-1} after 50 cycles. In addition, our described materials design for silicon-based anodes may be extended to other battery electrode material systems that experience large volume changes during cycling, such as sulfur.

Acknowledgements

The research was financially supported by the Programme for Changjiang Scholars and Innovative Research Team in University (IRT1177), the Foundation of Northwest Normal University (NWNU-LKQN-13-5), Key Laboratory of Eco-Environment-Related Polymer Materials of Ministry of Education and Key Laboratory of Polymer Materials of Gansu Province.

Notes and references

Key Laboratory of Eco-Environment-Related Polymer Materials of Ministry of Education, Key Laboratory of Polymer Materials of Gansu Province, College of Chemistry and Chemical Engineering, Northwest Normal University, Lanzhou 730070, China. E-mail: wangqt@nwnu.edu.cn; leizq@nwnu.edu.cn; Fax: +86 931 7971989; Tel.: +86 931 7971533

1 (a) M. Armand and J.-M. Tarascon, *Nature*, 2008, **451**, 652; (b) J. B. Goodenough and K. S. Park, *Journal of the American Chemical Society*, 2013, **135**, 1167.

2 M. Yoshio, H. Wang, K. Fukuda, T. Umeno, N. Dimov and Z. Ogumi, *Journal of The Electrochemical Society*, 2002, **149**, A1598.
3 (a) Y.-S. Hu, R. Demir-Cakan, M.-M. Titirici, J.-O. Müller, R. Schlögl, M. Antonietti and J. Maier, *Angewandte Chemie International Edition*, 2008, **47**, 1645; (b) U. Kasavajjula, C. Wang and A. J. Appleby, *Journal of Power Sources*, 2007, **163**, 1003.
4 L. Y. Beaulieu, K. W. Eberman, R. L. Turner, L. J. Krause and J. R. Dahn, *Electrochemical and Solid-State Letters*, 2001, **4**, A137.
5 J. H. Ryu, J. W. Kim, Y.-E. Sung and S. M. Oh, *Electrochemical and Solid-State Letters*, 2004, **7**, A306.
6 Y. Xu, G. Yin, Y. Ma, P. Zuo and X. Cheng, *Journal of Materials Chemistry*, 2010, **20**, 3216.
7 B. Wang, X. Li, T. Qiu, B. Luo, J. Ning, J. Li, X. Zhang, M. Liang and L. Zhi, *Nano letters*, 2013, **13**, 5578.
8 H. Wu, G. Chan, J. W. Choi, I. Ryu, Y. Yao, M. T. McDowell, S. W. Lee, A. Jackson, Y. Yang, L. Hu and Y. Cui, *Nature nanotechnology*, 2012, **7**, 310.
9 F. Xia, S. B. Kim, H. Cheng, J. M. Lee, T. Song, Y. Huang, J. A. Rogers, U. Paik and W. I. Park, *Nano letters*, 2013, **13**, 3340.
10 H. Li and H. Zhou, *Chemical communications*, 2012, **48**, 1201.
11 S. Guo, H. Li, H. Bai, Z. Tao and J. Chen, *Journal of Power Sources*, 2014, **248**, 1141.
12 M. A. Bangar, W. Chen, N. V. Myung and A. Mulchandani, *Thin Solid Films*, 2010, **519**, 964.
13 S. Y. Chew, Z. P. Guo, J. Z. Wang, J. Chen, P. Munroe, S. H. Ng, L. Zhao and H. K. Liu, *Electrochemistry Communications*, 2007, **9**, 941.
14 L. Pan, G. Yu, D. Zhai, H. R. Lee, W. Zhao, N. Liu, H. Wang, B. C.-K. Tee, Y. Shi, Y. Cui and Z. Bao, *Proceedings of the National Academy of Sciences*, 2012, **109**, 9287.
15 J.-J. Cai, P.-J. Zuo, X.-Q. Cheng, Y.-H. Xu and G.-P. Yin, *Electrochemistry Communications*, 2010, **12**, 1572.
16 Y. Yao, N. Liu, M. T. McDowell, M. Pasta and Y. Cui, *Energy & Environmental Science*, 2012, **5**, 7927.
17 S. E. Mavundla, G. F. Malgas, D. E. Motaung and E. I. Iwuoha, *Journal of Materials Science*, 2010, **45**, 3325.
18 J. Stejskal, M. Trchová, I. A. Ananieva, J. Janča, J. Prokeš, S. Fedorova and I. Sapurina, *Synthetic Metals*, 2004, **146**, 29.
19 C. Zhou, J. Han, G. Song and R. Guo, *Journal of Polymer Science Part A: Polymer Chemistry*, 2008, **46**, 3563.
20 V. Lim, E. Kang, K. Neoh, Z. Ma and K. Tan, *Applied surface science*, 2001, **181**, 317.
21 C. K. Chan, H. Peng, G. Liu, K. McIlwrath, X. F. Zhang, R. A. Huggins and Y. Cui, *Nature nanotechnology*, 2008, **3**, 31.
22 M. N. Obrovac and L. J. Krause, *Journal of The Electrochemical Society*, 2007, **154**, A103.
23 Y. M. Lee, J. Y. Lee, H.-T. Shim, J. K. Lee and J.-K. Park, *Journal of The Electrochemical Society*, 2007, **154**, A515.
24 J. Tu, L. Hu, W. Wang, J. Hou, H. Zhu and S. Jiao, *Journal of the Electrochemical Society*, 2013, **160**, A1916.
25 X.-y. Zhou, J.-j. Tang, J. Yang, J. Xie and L.-l. Ma, *Electrochimica Acta*, 2013, **87**, 663.
26 (a) M. Green, E. Fielder, B. Scrosati, M. Wachtler and J. S. Moreno, *Electrochemical and Solid-State Letters*, 2003, **6**, A75; (b) Y.-X. Yin, S. Xin, L.-J. Wan, C.-J. Li and Y.-G. Guo, *The Journal of Physical Chemistry C*, 2011, **115**, 14148.
27 R. Ruffo, S. S. Hong, C. K. Chan, R. A. Huggins and Y. Cui, *The Journal of Physical Chemistry C*, 2009, **113**, 11390.

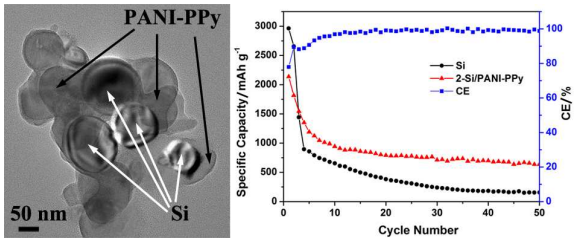

Poly(aniline-co-pyrrole) encapsulated Si nanoparticles composite anode material were prepared by *in situ* chemical oxidation polymerization method.